HHS Public Access

Author manuscript

Curr Drug Metab. Author manuscript; available in PMC 2022 January 01.

Published in final edited form as:

Curr Drug Metab. 2021 ; 22(9): 735–745. doi:10.2174/1389200222666210831125041.

Glutamine Antagonist GA-607 Causes a Dramatic Accumulation of FGAR which can be used to Monitor Target Engagement

Jesse Alt[1], **Sadakatali S. Gori**[1,2], **Kathryn M. Lemberg**[1,3], **Arindom Pal**[1,2], **Vijayabhaskar Veeravalli**[8], **Ying Wu**[1], **Joanna M.H. Aguilar**[1], **Ranjeet P. Dash**[1,2], **Lukáš Tenora**[9], **Pavel Majer**[9], **Qi Sun**[10], **Barbara S. Slusher**[1,2,3,4,5,6,7,*], **Rana Rais**[1,2,7,*]

[1] Johns Hopkins Drug Discovery, Johns Hopkins School of Medicine, Baltimore, MD 21205, USA

[2] Department of Neurology, Johns Hopkins School of Medicine, Baltimore, MD 21205, USA

[3] Department of Oncology, Johns Hopkins School of Medicine, Baltimore, MD 21205, USA

[4] Department of Psychiatry, Johns Hopkins School of Medicine, Baltimore, MD 21205, USA

[5] Department of Neuroscience, Johns Hopkins School of Medicine, Baltimore, MD 21205, USA

[6] Department of Medicine, Johns Hopkins School of Medicine, Baltimore, MD 21205, USA

[7] Department of Pharmacology and Molecular Sciences, Johns Hopkins School of Medicine, Baltimore, MD 21205, USA

[8] Drug Metabolism, Covance Laboratories Inc., Madison, WI 53704, USA

[9] Institute of Organic Chemistry and Biochemistry, Academy of Sciences of the Czech Republic v.v.i., Prague, 166 10, Czech Republic

[10] Jiangxi Science and Technology Normal University Nanchang, Jiangxi 330013, P.R. China

Abstract

[*] Address correspondence to these authors at the Johns Hopkins Drug Discovery, 855 North Wolfe Street, Baltimore, Maryland, 21205, USA; Tel: 410-614-0662; Fax: 410-614-0659; bslusher@jhmi.edu, Tel: 410-502-0497; rrais2@jhmi.edu.

CONFLICT OF INTEREST

The authors declare the following competing financial interest(s): Under a license agreement between Dracen Pharmaceuticals, Inc. and the Johns Hopkins University, Barbara S. Slusher, Rana Rais, and Jesse Alt, are entitled to royalty distributions related to technology used in the research described in this publication. Barbara S. Slusher, Pavel Majer, and Rana Rais, are also co-founders of and hold equity in Dracen Pharmaceuticals, Inc. which is clinically developing GA prodrugs. This arrangement has been reviewed and approved by the Johns Hopkins University in accordance with its conflict of interest policies.

ETHICS APPROVAL AND CONSENT TO PARTICIPATE

The protocol of this study was approved from John Hopkins University Animal Care and Use Committee (ACUC), USA (Approval no. MO19M27).

HUMAN AND ANIMAL RIGHTS

No humans were used for studies that are base of this research. Animals studies were carried out under the John Hopkins University Animal Care and Use Committee (ACUC) protocol as stated above.

CONSENT FOR PUBLICATION

Not Applicable.

AVAILABILITY OF DATA AND MATERIALS

The datasets generated and analyzed during the current study are available from the corresponding author [RR] on reasonable request.

SUPPLEMENTARY MATERIAL

Supplementary material is available on the publisher’s website along with the published article.

Background: Metabolomic analyses from our group and others have shown that tumors treated with glutamine antagonists (GA) exhibit robust accumulation of formylglycinamide ribonucleotide (FGAR), an intermediate in the *de novo* purine synthesis pathway. The increase in FGAR is attributed to the inhibition of the enzyme FGAR amidotransferase (FGAR-AT) that catalyzes the ATP-dependent amidation of FGAR to formylglycinamidine ribonucleotide (FGAM). While perturbation of this pathway resulting from GA therapy has long been recognized, no study has reported systematic quantitation and analyses of FGAR in plasma and tumors.

Objective: Herein, we aimed to evaluate the efficacy of our recently discovered tumor-targeted GA prodrug, GA-607 (isopropyl 2-(6-acetamido-2-(adamantane-1-carboxamido)hexanamido)-6-diazo-5-oxohexanoate), and demonstrate its target engagement by quantification of FGAR in plasma and tumors.

Methods: Efficacy and pharmacokinetics of GA-607 were evaluated in a murine EL4 lymphoma model followed by global tumor metabolomic analysis. Liquid chromatography-mass spectrometry (LC-MS) based methods employing the ion-pair chromatography approach were developed and utilized for quantitative FGAR analyses in plasma and tumors.

Results: GA-607 showed preferential tumor distribution and robust single-agent efficacy in a murine EL4 lymphoma model. While several metabolic pathways were perturbed by GA-607 treatment, FGAR showed the highest increase qualitatively. Using our newly developed sensitive and selective LC-MS method, we showed a robust >80- and >10-fold increase in tumor and plasma FGAR levels, respectively, with GA-607 treatment.

Conclusion: These studies describe the importance of FGAR quantification following GA therapy in cancer and underscore its importance as a valuable pharmacodynamic marker in the preclinical and clinical development of GA therapies.

Keywords

Glutamine antagonist; purine synthesis; formylglycinamide ribonucleotide; formylglycinamidine ribonucleotide; biomarker; cancer; LC-MS

1. INTRODUCTION

Purine nucleotide synthesis generates building blocks for DNA, RNA, high-energy intermediates, and signaling molecules in live cells. New purines can be generated by recycling turnover products in salvage pathways or synthesized *de novo* in a highly conserved ten-step pathway that transforms phosphoribosylpyrophosphate to inosine-5'-monophosphate [1]. Purine synthesis is an essential target in diseases, including viral infections, gout, and cancer [2–6]. Thus, the ability to accurately monitor the effects of purine synthesis blockade is of general interest.

FGAR is an intermediate metabolite at the fourth step of *de novo* purine synthesis. FGAR is a substrate for the enzyme formylglycinamide ribonucleotide amidotransferase (FGAR-AT, also known as phosphoribosylformylglycinamidine synthase or PFAS). Biochemical studies on prokaryotic homologues provide evidence for FGAR-AT catalyzed hydrolysis of glutamine to ammonia and glutamate; subsequently, ATP activates FGAR for

nucleophilic attack by the ammonia generated in the first half of the reaction to produce formylglycinamidine ribonucleotide (FGAM) [7]. Small molecule glutamine antagonists (GAs), including the irreversible inhibitor 6-diazo-5-oxo-L-norleucine (DON), target this conversion of FGAR to FGAM. In mammalian cell extracts enriched for FGAR-AT activity, the inhibitor constant (K_i) for DON was determined to be 1.1×10^{-6} M [8]. Classic studies with the incorporation of ^{14}C-formate into newly synthesized purines in leukemia cells grown in the presence and absence of GA revealed shifts in the HPLC profile of labeled compounds, including significant increases in the peaks corresponding to FGAR when a GA was present [9]. More recently, there has been interest in establishing nonradioactive analytical methods to detect FGAR and other *de novo* purine synthesis intermediates from human tissue or bio-fluid samples to screen purine synthesis gene products where metabolic causes of disease were not known. To this end, elevation in FGAR levels in human tissue samples was evaluated using an Orbitrap Elite mass spectrometer *via* MS^2 fragmentation analysis followed by confirmation with an FGAR standard synthesized from bacterial recombinant enzymes [10].

Recently, there has been renewed interest in GA as a therapeutic strategy for cancer [11–15]. Blockade of glutamine utilization using a broadly active small molecule GA induces divergent metabolic programs in cancer cells *versus* effector T-cells, which ultimately results in the ability to overcome tumor immune evasion [13]. Also, myeloid-derived suppressor cells (MDSCs) play important roles in creating an immunosuppressive tumor microenvironment [16] and express enzymes that deplete key nutrients from T-cells. Our previous report revealed that blocking glutamine metabolism markedly inhibits the generation and recruitment of MDSCs [17]. Unfortunately, there are no broadly active GAs available clinically; DON was evaluated in oncology patients several decades ago, but its development was halted due to excessive gastrointestinal toxicity [18]. Our group has recently discovered a tumor-targeted prodrug strategy for DON, designed to mask the active compound with pro-moieties, which are hydrolyzed by tumorenriched enzymes for bioactivation. One of our lead compounds, termed GA-607 (isopropyl 2-(6-acetamido-2-(adamantane-1-carboxamido)hexanamido)-6-diazo-5-oxohexanoate; comp. **6** in [11]) showed a remarkable 11-fold higher DON exposure to tumor (target tissue) *versus* GI tissues (toxicity tissue) [11]. However, its *in vivo* efficacy and target engagement in murine models was not established. Moreover, the effect of GA-607 on the *de novo* purine synthesis pathway, specifically FGAR, was not determined due to lack of a selective and sensitive bioanalytical method applicable in plasma and tumor samples.

Herein, we report that GA-607 has robust single-agent efficacy in mice bearing EL4 tumors. Using metabolomics, we demonstrate that the purine precursor FGAR as well as other metabolites, are significantly affected by GA in tumors. We developed a novel LC-MS method for the quantitation of FGAR in biological tissues and showed robust accumulation of FGAR in tumors and plasma following GA-607 treatment. This new bioanalytical method could have utility in quantifying FGAR levels as a target engagement biomarker for treatment modalities such as GA-607 that cause inhibition of purine biosynthesis and thus could aid in their clinical development.

2. MATERIALS AND METHODS

2.1. Reagents and Chemicals

GA-607 was synthesized as previously reported [11]. FGAR was provided as a generous gift from Dr. Qi Sun, Laboratory of Organic Chemistry, Jiangxi Science and Technology Normal University (Nanchang, China). Deuterated *N*-acetyl-L-aspartic acid (NAA-d_3; internal standard) was obtained from Canadian Isotopes (Quebec, Canada). LC-MS-grade water, methanol, acetonitrile, and formic acid were obtained from Thermo Fisher Scientific (Waltham, MA, USA). *N,N*-Dimethylhexylamine (DMHA) was obtained from Sigma Aldrich (St. Louis, MO, USA).

2.2. Evaluation of Efficacy and Pharmacokinetics of GA-607 in Mice Bearing EL4 Flank Tumors

All animal studies were conducted in accordance with the protocols reviewed and approved by the Johns Hopkins Institutional Animal Care and Use Committee in compliance with the Association for Assessment and Accreditation of Laboratory Animal Care International and the Public Health Service Policy on the Humane Care and Use of Laboratory Animals (PHS Policy). Efficacy evaluation was conducted in C57BL/6 CES1$^{-/-}$ mice bearing EL4 lymphoma tumors. Tumors were grafted in mice as described previously with minor modifications [11]. Briefly, mice weighing between 25–30 g and 6–8 weeks of age were maintained on a 12 h light-dark cycle, with access to food and water, *ad libitum*. EL4 mouse lymphoma cells were obtained as a gift from Dr. Jonathan Powell's laboratory (Johns Hopkins University, Baltimore, MD). Cells were maintained in RPMI 1640 medium with FBS 10% (v/v), antimycotic/antibiotic 1% (v/v), 2 mM of L-glutamine and 10 mM HEPES in a 5% (v/v) CO_2 and 95% (v/v) air incubator.

Upon confluency, mice were injected with EL4 cells (0.3×10^6 cells in 0.2 mL of phosphate-buffered saline, pH 7.4) in one location on the flank. Mice whose tumors reached a mean volume of ~400 mm^3 (approximately 7 days post-inoculation) were used for the efficacy study. Mice (n=12/group) were randomized into vehicle-treated or GA-607-treated (3.2 mg/kg of GA-607, equivalent to 1 mg/kg DON) groups, and dosed once daily subcutaneously (SC) in ethanol/tween 80/saline (5:10:85 v/v/v) for 5 consecutive days per week (with a 2-day break in dosing); a regimen which was previously shown to be tolerable and effective with other glutamine antagonists [13]. Tumor volume and body weight were measured and recorded on the days the mice were dosed.

We also assessed the pharmacokinetics of GA-607 and subsequent DON release in a satellite cohort bearing the EL4 tumor. Prior to dosing, the interscapular region of the mice was wiped with alcohol gauze. GA-607 was dissolved immediately (ethanol/tween 80/saline (5:10:85 v/v/v) and was administered to mice as a single SC dose of 3.2 mg/kg (1 mg/kg DON equivalent dose). The mice were euthanized with carbon dioxide at 1 h and 4 h post-drug administration; blood samples (~0.8 mL) were collected in heparinized microtubes by cardiac puncture, and tumors were removed and flash-frozen on dry ice. Blood samples were centrifuged at a temperature of 4°C at 3000 *g* for 10 min. All samples were kept chilled throughout processing. Plasma samples (0.3 mL) were collected in polypropylene tubes and

stored at −80°C until bioanalysis. Flash-frozen tumor samples also were stored at −80°C until bioanalysis.

Bioanalysis of the pharmacokinetic samples was performed as previously described [11]. For quantifying the intact GA-607, standards (0.001–50 nmol/mL), QCs and samples were protein precipitated by adding 5 μL of methanol containing internal standards (losartan: 0.5 μM and 10 μM glutamate-d_5) per milligram of tissue, followed by homogenization (tumor tissue) or vortex-mixing (plasma) and then centrifugation at 16,000 *g* for 5 min at 4°C. Then, 2 μL of the supernatant was injected into the LC-MS/MS system. The $[M+H-N_2]^+$ ion transition of GA-607 (m/z 518.142 →153.976, 500.401) and $[M+H]^+$ ion transitions of losartan (IS) (m/z 422.938 → 184.580, 209.275) were used.

For the bioanalysis of DON, the supernatants (100 μL) were transferred to fresh tubes and dried under vacuum at 45°C for 1 h. To each tube, 50 μL of 0.2 M sodium bicarbonate buffer (pH 9.0) and 100 μL of 10 mM dabsyl chloride were added. After vortex-mixing, samples were incubated at 60°C for 15 min to derivatize, followed by centrifugation at 16,000 *g* for 5 min at 4°C. The supernatants (20 μL) were transferred to a 96-well plate, diluted with 80 μL of water and injected onto LC-MS/MS. Quantification was performed in parallel-reaction monitoring mode as previously described [11, 19].

2.3. Metabolomic Analysis of Mice Following GA-607 Therapy

C57BL/6 CES1$^{-/-}$ mice (n=5/group) bearing flank EL4 tumors were treated with either vehicle or GA-607 (3.2 mg/kg; 1 mg/kg DON equivalent dose); the groups were dosed SC once a day for 4 days until a significant reduction in tumor growth was observed in GA-607 group (tumors still present in sufficient quantity for analyses). One hour after the dose on day 4 mice were euthanized, and tumor tissues were harvested and then flash-frozen in liquid nitrogen. Tumor processing for metabolomics was performed as previously described [15, 17]. Briefly, tumors were homogenized by sonication in 80% cold methanol. Samples were vortexed and stored at −80°C overnight to precipitate proteins, then centrifuged at 16,000 *g* for 10 minutes. Supernatants were dried under a steady stream of nitrogen gas and reconstituted in 50% acetonitrile. Samples were analyzed using an Agilent 1290 Infinity Binary UHPLC pump with well-plate autosampler at 4°C and an Agilent 6520 Q-TOF MS. Chromatography was performed following injection of 4 μL samples over a Zorbax Extend C18 column at 40°C by gradient elution run from 3% methanol with 5 mmol/L tributylamine to 100% methanol with 5 mmol/L tributylamine over 22 minutes. The MS was equipped with a dual electrospray ion source operated in negative-ion mode. Data were acquired with Agilent MassHunter Acquisition software and processed using MassHunter Qualitative Analysis software and MAVEN [20]. Metabolite identification was performed using mass-to-charge ratio and retention times from known standards or fragmentation analysis. Metabolite peak areas were normalized to extracted tumor weights. Statistical tests for the volcano plot were performed in Excel.

2.4. Ion-exchange LC-MS Method for FGAR Quantification

Various chromatographic conditions were evaluated initially, including hydrophilic interaction liquid chromatography (HILIC), reverse phase (C8, C18, Hypersil BDS)

chromatography, and multiple mobile phase combinations for achieving optimal chromatographic separation and sensitivity for FGAR. However, an ion-pairing chromatography approach consisting of DMHA as an aqueous and organic modifier in water and acetonitrile, respectively, and a reverse phase C18 HPLC column gave optimal peak shape and retention. Due to the unavailability of isotopic analogue of FGAR, a stable isotope-labeled deuterated analogue of *N*-acetyl aspartic acid (NAA-d_3) was selected as the internal standard, as under these ion-pair chromatographic conditions, NAA-d_3 exhibited similar retention time to FGAR as well as a good chromatographic peak shape and MS signal, and was deemed suitable for quantification of FGAR.

2.4.1. Calibration Standards and Quality Control Samples—The FGAR standard was characterized by NMR and high-resolution mass spectroscopy (supporting Figs. S1–S4). A 100 mM stock solution of FGAR was prepared in water and stored at −20°C. All calibration standards and quality control (QC) samples of FGAR were prepared fresh each day before analysis. The working solutions were prepared by serial dilution in the extraction solvent (10 μM deuterated NAA-d_3 in methanol). Calibration standards for FGAR were prepared in plasma (0.03–100 nmol/mL) and tumors (1–1000 nmol/g). Similarly, quality control (QC) samples were prepared independently at three concentrations in plasma (0.08, 2, 80 nmol/mL) and tumor homogenate (20, 200, 2000, nmol/g) covering low, medium and high concentrations levels. Calibration curve fit obtained from peak area ratio (area of analyte/area of internal standard), was assessed by weighted ($1/\text{concentration}^2$) quadratic non-linear regression. For tumor analyses, the standard curve was fitted using a blank subtraction method as reported previously [21] to compensate for the presence of endogenous FGAR levels. This was important as it allowed the use of tumor matrix for the calibration while maintaining the recovery and matrix effects between samples and calibration curves. Using this method, LLOQ was determined by *t*-test and defined as the minimum concentration that resulted in a statistically significant increase above the background [22]. The concentration of each standard was back-calculated from calibration curve parameters, and concentrations in QC, and unknown samples were determined by interpolation. The calibration curve correlation coefficients (R^2) ≥0.990 were considered acceptable for all analytical runs. The acceptance criteria for each back-calculated standard concentration was set at ±15% deviation from the nominal value except at the LLOQ, which was set at ±20%.

2.4.2. Chromatographic and Mass Spectrometric Conditions—Samples were analyzed using UltiMate 3000 UHPLC coupled to Q Exactive Focus Orbitrap Mass Spectrometer (Thermo Fisher Scientific Inc., Waltham, MA, USA). The mobile phase used for chromatographic separation consisted of 8 mM DMHA + 0.005% formic acid in water, pH 9 (A), and 8 mM DMHA in acetonitrile (B), delivered at a flow rate of 0.4 mL/min. A gradient LC method (time (min)/%B: 0–0.5/5, 2.5–3.5/95, 3.51–4.50/5) with a short runtime of 4.5 min was developed for the analyses. Separation of analytes was achieved at room temperature using an Agilent Eclipse Plus C18 RRHD 2.1 × 100 mm, 1.8 μm particle size column (Agilent, Santa Clara, CA, USA). Samples were introduced to the interface through a heated ion spray with the capillary temperature setting at 350°C and a spray voltage of 4 kV. Nitrogen was used as the sheath and auxiliary gas set to 30 and 20 arbitrary units,

respectively. Samples were subjected to ionization in negative mode and analyzed using the Full MS scan function. Parent ion of FGAR at m/z 313.0442 was used for quantitation and parent ion of NAA-d_3 at m/z 177.0596 was used as an internal standard. Data were acquired and quantified with Xcalibur 4.1.31.9.

2.5. Method Validation

The intra-day and inter-day precision and accuracy for QC samples in both plasma and tumor were determined (for inter-day, n=3/day over 2 days), and statistical estimates were tabulated. Extraction efficiency, matrix effect as well as bench-top, freeze-thaw, long-term, and autosampler stability were also evaluated in triplicate at each QC level. Extraction efficiency was calculated by comparing mean peak responses obtained from pre-spiked samples against post-spiked samples. Matrix effect was evaluated from mean peak responses obtained from post-spiked samples compared to neat standards prepared in the extraction solvent. For stability assessment, spiked samples were a) freeze-thawed for three cycles (freeze-thaw stability), b) left at room temperature for 6 h (benchtop stability) or c) frozen at −80°C for 4 weeks before extraction (long-term stability). The autosampler stability was evaluated at 4°C by analyzing QC samples immediately after extraction and after 18 h storage in the autosampler. Regardless of the type of stability experiments conducted, the bias was contained within 85–115% of the nominal values and the precision within ±15% RSD. Assessment of carryover between autosampler injections was made by injecting a double blank sample after the upper limit of quantitation standard in calibration curve (100 nmol/mL in plasma; 10000 nmol/g in tumor). For analyte, carry over in the blank sample following the ULOQ standard should not be greater than 20% of the LLOQ, whereas, for the internal standard, the response in the blank sample should not exceed 5% of the average internal standard response of the calibrators and QCs.

2.6. Quantification of FGAR in Plasma and Tumor Samples

Mice (n=6/group) were randomized into vehicle-treated or GA-607-treated (3.2 mg/kg; 1 mg/kg DON equivalent dose) groups, and were dosed SC once a day for four days. The mice were sacrificed on day 4, and both plasma and tumor samples were collected (1 and 4h post dose) and frozen at −80°C for FGAR bioanalysis.

Prior to extraction, frozen samples of plasma and tumor were thawed on ice. Sample preparation was performed using a single-step protein precipitation method. For plasma, extraction of analyte was conducted using 20 μL of the sample with 100 μL of extraction solvent (methanol containing 10 μM deuterated *N*-Acetyl Aspartic acid (NAA-d_3) as internal standard), followed by vortex mixing for 30 s and centrifugation at 16,000 *g* for 5 min at 4°C. The resulting supernatants were transferred to a 96-well plate and analyzed by LC-MS. Similarly, for tumor, ~50 mg of EL4 tumor samples were processed by the addition of 5 μL extraction solvent per each mg of tissue and homogenized with Spex® 2150 stainless steel beads at 1500 rpm for 3 min on Spex® Geno/Grinder® (Spex SamplePrep LLC, Metuchen, NJ, USA). Post homogenization, samples were centrifuged at 16,000 *g* for 5 min at 4°C, and supernatants were diluted 5-fold in water and analyzed using the LC-MS method described above.

2.7. Statistical Analysis

For biomarker comparisons, groups were statistically compared by one-way ANOVA with Tukey's post hoc test. The *a priori* level of significance for all analyses was defined as $p < 0.05$.

3. RESULTS AND DISCUSSION

Amongst the GAs reported to-date, DON has been the most extensively studied both preclinically and in clinical trials [23–25]. DON is structurally similar to L-glutamine and broadly inhibits glutamine-utilizing enzymes involved in purine and pyrimidine synthesis, co-enzyme synthesis, amino acid synthesis, and hexosamine production [26]. DON has been evaluated in human studies since the 1950s and was found to elicit a favorable response in cancer patients, however, its efficacy was marred by its toxicity resulting from local glutamine starvation in the gastrointestinal (GI) tract [23, 27–31]. We have previously reported the development of DON prodrugs that preferentially target the tumor environment [11, 13, 32, 33]. One of our lead compounds, GA-607 (Fig. (1A), demonstrated stability in blood and excellent permeability into the tumor where it is selectively transformed to DON. Herein, we first evaluated the efficacy and exposures of GA-607 in a murine EL4 lymphoma model followed by metabolomic analysis to reveal its perturbations of metabolic pathways. Considering the dramatic qualitative increase observed in FGAR (Fig. (1B) levels, we developed a sensitive and robust bioanalytical method to evaluate the target engagement of GA-607 by quantitation of FGAR.

The efficacy of GA-607 was assessed in C57BL/6 $CES1^{-/-}$ mice bearing EL4 lymphoma tumors at 3.2 mg/kg SC (1 mg/kg DON equivalent dose). Our previous published report revealed that this dosing regimen afforded an ideal pharmacokinetic profile [11], releasing efficacious levels of DON within the tumor. As shown in (Fig. (2A), the vehicle-treated mice showed continued tumor growth over time, while the mice treated with GA-607 had complete tumor regression. Furthermore, no changes were observed in the body weight (Fig. (2B), general appearance, and behavior, demonstrating the efficacy of GA-607 with good tolerability.

In addition to efficacy evaluation, drug exposures were also quantified in plasma and tumor tissue for confirmation of tumor distribution. The data obtained from a satellite cohort (Fig. (2C and D) showed preferential DON delivery to the tumor. The intact levels of the GA-607 in plasma were approximately 160 nM at 1-hour post-dose but were below the limit of quantification at 4 hours post-dose (Fig. (2C). The GA-607-derived DON levels in the tumor were approximately 5-fold higher than that of plasma (3.1 μM *versus* 0.651 μM at 1 h post-dose) (Fig. (2D). A similar 5-fold higher DON tumor exposure was also observed at 4 h (0.75 μM *versus* 0.16 μM).

We next conducted global metabolomic analysis in tumors treated with GA-607. Fifty polar metabolites were queried based on mass-to-charge ratio and retention times, and twenty-nine of those were identified among the analyzed samples. Notably, the metabolite with the greatest increase upon GA-607 treatment was FGAR (ratio GA-607/vehicle = 244.96, p-value = 0.0045) (Fig. (3). Other metabolites that demonstrated significant

modulation upon GA-607 treatment are also noted in (Fig. (3). Consistent with prior studies and the known direct biochemical effect of GA-607, glutamine was also increased (ratio GA-607/vehicle = 5.21, p-value 0.0017). Other significantly modulated metabolites are in pathways containing glutamine amidotransferases including uridine 5′-diphospho-N-acetylglucosamine (UDP-GlcNAc) in hexosamine metabolism, nucleotide diphosphates (guanosine diphosphate (GDP), cytidine diphosphate (CDP), and uridine diphosphate (UDP)) in nucleotide metabolism, and aspartate in amino acid metabolism. Considering the role of FGAR in purine synthesis and its robust modulation upon glutamine antagonism, we focused on development of a sensitive and selective LC-MS assay for FGAR and used it to quantitatively monitor changes in plasma and tumors following GA-607 treatment.

While previous reports of FGAR are qualitative in nature [9, 10], recently Krijt *et al.,* reported an LC-MS/MS-based bioanalytical assay for the quantification of FGAR [34, 35]. However, this method is limited in utility as it has only been tested in urine, dried blood spots and *in vitro* cultures. The sensitivity of this method has not been evaluated in more complex biomatrices such as plasma and tumor homogenates, as reported here. Furthermore, the method required extensive equilibration time and column regeneration after each run, thus requiring 25 min of runtime for each sample; this severely limits the throughput capacity of the method. We developed a full scan MS analysis using a high-resolution Q Exactive Orbitrap mass spectrometer that provides accurate detection of masses within 2 ppm error with the total runtime of only 4.5 min per sample. The LLOQ for FGAR in plasma was established at 0.03 nmol/mL with an accuracy of 99.0% and precision ≤5.09% (n=6). For determination of LLOQ in tumors we employed a blank subtraction method during data analyses [21]. Tumors have been reported to have baseline levels of endogenous FGAR [36] and simple linear regression without subtraction of endogenous levels would have resulted in erroneous results. Furthermore, this approach also allowed the use of tumor matrix for calibration standards without compromising the recovery or causing differential matrix effects [37–39]; the limitations often encountered when using surrogate matrices. Using this method, the LLOQ for FGAR in the tumor was determined to be 1 nmol/g, as this was the lowest standard concentration that showed statistically significant difference from the background levels ($p < 0.05$), as determined by *t*-test [22]. More importantly, the higher LLOQ in tumor *versus* plasma was not because of the lack of sensitivity of the analytical method, but due to the high endogenous levels of FGAR in tumor. The LLOQ for FGAR in the tumor homogenate exhibited an accuracy and precision of 99.6% and 3.63%, respectively (n=6). Due to a positive parabolic (non-linear) mass spectrometer response observed with increasing concentrations of the FGAR standards across a wide calibration range (0.03–100 nmol/mL in plasma, 1–1000 nmol/g in tumor), a linear regression was unsuitable, and a quadratic fit offered the desired precision and accuracy for the calibration standards [40–42]. Curve fit in plasma and tumor homogenates provided a correlation coefficient of greater than 0.995 ± 0.003 (n=6) and 0.994 ± 0.007 (n=6), respectively. High-resolution mass spectrum and representative chromatographic spectra of FGAR and IS (NAA-d_3) in plasma and tumor samples are shown in (Fig. (4). Back-calculated concentrations for the calibration standards in plasma and tumor homogenates obtained from regression analysis were within 94.4–105 % and 93.0–104 %, respectively (Table 1).

Extraction efficiency for FGAR quantification was determined by the relative recovery of FGAR extracted from plasma compared to post extraction-spiked samples and ranged from 85% to 99%, with an average of 89%. Similarly, the extraction efficiency of FGAR from the tumor homogenates ranged from 99% to 104%, with an average of 103%. The results obtained from stability experiments are presented in Tables 2 and 3 for plasma and tumor homogenates, respectively. FGAR was found to be stable at all the tested conditions (freeze-thaw/bench-top/long-term/autosampler) with a <15% deviation from nominal concentrations in both plasma and the tumor homogenates. Matrix effect, as determined by the FGAR peak area between post-extraction spiked and neat standards, ranged from −18% to 6% with an average of −14% in plasma, and ranged from −6% to 17% with an average of 8% in tumor homogenates, and was within the acceptable limits of ± 20% at all tested concentrations. A blank injection following a high standard of 100 nmol/mL in plasma, revealed a minimal carry-over area of 8.97% of the LLOQ standard, which was within the acceptable range. Similarly, carryover in tumor homogenate samples was estimated to be 7.25%. No carry-over was observed for the internal standard. Inter-day accuracy, and precision (%RSD) of QC's (n=3/day; 2 days) in plasma ranged from 91.0–99.4% and 4.82–13.6%, respectively (Table 4). Likewise, inter-day accuracy and precision (n=3/day; 2 days) for QC's in the tumor homogenates ranged from 98.1–104% and 4.03–6.03%, respectively (Table 5). These results indicate that the LC-MS method developed is robust, precise, and accurate for the quantitation of FGAR in both plasma and tumor.

FGAR quantification was performed in samples collected after 4 days of GA-607 administration when significant tumor suppression was observed. In the tumors of vehicle-treated mice, an average of 16 and 15 nmol/g FGAR was quantified at 1 h and 4 h post-dose, respectively. In contrast, GA-607 treated animals showed a remarkable 1300 and 1600 nmol/g FGAR at 1 and 4 h post-dose, respectively. These levels represent an 80- to 100-fold increase (Fig. 5A-ii). In contrast, in plasma of GA-607 treated mice, much lower levels were observed (0.3 and 0.5 nmol/mL at 1 and 4 h post-dose, respectively) compared to tumor; however, these levels were still >10-fold higher when compared to vehicle-treated animals, which were generally below the limit of quantification (<0.03 nmol/mL) (Fig. 5A-i). These data support the target engagement of GA-607 to FGAR-AT as presented in Fig. (5B) schematic. Thus, FGAR could be used as a biomarker of the GA-607 effect.

The FGAR quantification method presented here is a sensitive and selective LC-MS method for direct analysis of FGAR in plasma and tumors. The presented data also makes a strong case for FGAR modulation to corroborate the target engagement of glutamine antagonists. With the prodigious efforts being poured into the discovery and development of glutamine antagonists for the treatment of cancer and other diseases [32, 43–45], development of a biomarker such as FGAR may serve as a valuable tool in both diagnosing dysfunctions in this pathway as well as assessing the target engagement of therapies focused on modulating nucleotide synthesis. Also, while the focus of this report was to demonstrate the efficacy of GA-607 and the identification of FGAR as a target engagement tool, future efforts will be focused on evaluating the effects on downstream metabolites such as FGAM and their quantification. Importantly, although current studies report the evaluation of GA-607 only in EL4 tumor model, we have previously studied our novel GA prodrugs in multiple tumor types (*e.g.* MC38 colon cancer, CT26 colon cancer, B16 melanoma, 4T1 mammary cancer)

with various dosing regimens and treatments when the tumors were small (~30 mm^3) as well as large (~300 mm^3) and as both single agents and in combination with immunotherapies [13, 15, 17]. Furthermore, our lead glutamine antagonist, DRP-104, is currently in phase I clinical trial (*Clinical Trial Identifier:* NCT04471415) for advanced solid tumors and has received a fast-track FDA designation for the treatment of advanced non-small-cell lung carcinoma (NSCLC) [46]. These studies underscore the broad applicability of GA therapy to various tumor types and the importance of a biomarker/target engagement tool, such as FGAR that may aid in the further development of these analogs as anticancer agents.

CONCLUSION

The tumor-targeted glutamine antagonist GA-607 was shown, for the first time, to have robust single-agent tumor regression activity in a murine EL4 lymphoma tumor model without any observable signs of toxicity. Metabolomic analyses revealed that GA-607 caused dramatic FGAR accumulation in addition to perturbing other known glutamine-utilizing pathways. A new rapid, sensitive, selective, and reliable LC-MS method was developed and optimized for the quantification of FGAR in plasma and tumor using an *N,N*-dimethylhexylamine assisted ion-pairing chromatography approach. The method demonstrated good sensitivity, precision, accuracy, and recovery in both plasma and tumor samples. Further, the application of the method to monitor target engagement was demonstrated using GA-607 treatment in EL4 tumored mice. We propose FGAR as a promising pharmacodynamic marker that can quantitatively reveal dysfunction in *de novo* purine synthesis and validate the target engagement of therapeutic modalities targeting the pathway. Moreover, while studies reported here were limited to only EL4 tumors, the FGAR quantification method described will be broadly applicable to multiple tumor types sensitive to glutamine antagonism in preclinical models and ultimately in clinical studies.

Supplementary Material

Refer to Web version on PubMed Central for supplementary material.

ACKNOWLEDGEMENTS

The authors thank Dr. Jonathan Powell's Laboratory (Johns Hopkins University, Baltimore, MD) for the generous gift of EL4 mouse lymphoma cells.

FUNDING

This research was supported by NIH Grant R01CA193895 (to B.S.S. and R.R.), R01CA229451 (to B.S.S. and R.R.), Bloomberg Kimmel Institute for Cancer Immunotherapy (to B.S.S. and R.R.), LTAUSA18166 by the Ministry of Education, Youth and Sports of the Czech Republic (program INTER-EXCELLENCE to P.M.), and by the Institute of Organic Chemistry and Biochemistry of the Academy of Sciences of the Czech Republic, v.v.i. (RVO 61388963). K.M.L. was supported by a CureSearch Young Investigator Award.

LIST OF ABBREVIATIONS

AUC	Area Under Curve
CES1$^{-/-}$	Carboxylesterase 1 Knockout

DMHA	N,N-dimethylhexylamine
DON	6-diazo-5-oxo-L-norleucine
FGAM	Formylglycinamidine Ribonucleotide
FGAR	Formylglycinamide Ribonucleotide
FGAR-AT	Formylglycinamide Ribonucleotide Amidotransferase
GA	Glutamine Antagonist
HILIC	Hydrophilic Interaction Liquid Chromatography
LC-MS	Liquid Chromatography-mass Spectrometry
LLOQ	Lower Limit of Quantitation
NAA-d_3	N-acetyl Aspartate Deuterated
QC	Quality Control
SC	Subcutaneous
UHPLC	Ultra-high Performance Liquid Chromatography

REFERENCES

[1]. Pedley AM; Benkovic SJ A new view into the regulation of purine metabolism: The purinosome. Trends Biochem. Sci, 2017, 42(2), 141–154. 10.1016/j.tibs.2016.09.009 PMID: 28029518 [PubMed: 28029518]

[2]. Yin J; Ren W; Huang X; Deng J; Li T; Yin Y Potential mechanisms connecting purine metabolism and cancer therapy. Front. Immunol, 2018, 9, 1697. 10.3389/fimmu.2018.01697 PMID: 30105018 [PubMed: 30105018]

[3]. Wang Y; Wang W; Xu L; Zhou X; Shokrollahi E; Felczak K; van der Laan LJ; Pankiewicz KW; Sprengers D; Raat NJ; Metselaar HJ; Peppelenbosch MP; Pan Q Cross talk between nucleotide synthesis pathways with cellular immunity in constraining hepatitis E virus replication. Antimicrob. Agents Chemother, 2016, 60(5), 2834–2848. 10.1128/AAC.02700-15 PMID: 26926637 [PubMed: 26926637]

[4]. Aleo F The hormonal regulation of purine biosynthesis: basal levels of different hormones in primary gout. Adv. Exp. Med. Biol, 1984, 165(Pt A), 437–440.

[5]. Hershfield MS; Seegmiller JE Gout and the regulation of purine biosynthesis. Horiz. Biochem. Biophys, 1976, 2, 134–162. PMID: 776767 [PubMed: 776767]

[6]. Grayzel AI; Seegmiller JE; Love E Suppression of uric acid synthesis in the gouty human by the use of 6-diazo-5-oxo-L-norleucine. J. Clin. Invest, 1960, 39, 447–454. 10.1172/JCI104057 PMID: 13829149 [PubMed: 13829149]

[7]. Hoskins AA; Anand R; Ealick SE; Stubbe J The formylglycinamide ribonucleotide amidotransferase complex from *Bacillus subtilis*: metabolite-mediated complex formation. Biochemistry, 2004, 43(32), 10314–10327. 10.1021/bi049127h PMID: 15301530 [PubMed: 15301530]

[8]. Levenberg B; Melnick I; Buchanan JM Biosynthesis of the purines. XV. The effect of aza-L-serine and 6-diazo-5-oxo-L-norleucine on inosinic acid biosynthesis *de novo*. J. Biol. Chem, 1957, 225(1), 163–176. 10.1016/S0021-9258(18)64919-1 PMID: 13416227 [PubMed: 13416227]

[9]. Lyons SD; Sant ME; Christopherson RI Cytotoxic mechanisms of glutamine antagonists in mouse L1210 leukemia. J. Biol. Chem, 1990, 265(19), 11377–11381. 10.1016/S0021-9258(19)38603-X PMID: 2358467 [PubMed: 2358467]

[10]. Mádrová L; Krijt M; Barešová V; Václavík J; Friedecký D; Dobešová D; Součková O; Škopová V; Adam T; Zikánová M Mass spectrometric analysis of purine de novo biosynthesis intermediates. PLoS One, 2018, 13(12), e0208947. 10.1371/journal.pone.0208947 PMID: 30532129 [PubMed: 30532129]

[11]. Tenora L; Alt J; Dash RP; Gadiano AJ; Novotna K; Veeravalli V; Lam J; Kirkpatrick QR; Lemberg KM; Majer P; Rais R; Slusher BS Tumor-targeted delivery of 6-diazo-5-oxo-l-norleucine (DON) using substituted acetylated lysine prodrugs. J. Med. Chem, 2019, 62(7), 3524–3538. 10.1021/acs.jmedchem.8b02009 PMID: 30892035 [PubMed: 30892035]

[12]. Wang SZ; Poore B; Alt J; Price A; Allen SJ; Hanaford AR; Kaur H; Orr BA; Slusher BS; Eberhart CG; Raabe EH; Rubens JA Unbiased metabolic profiling predicts sensitivity of high MYC-expressing atypical teratoid/rhabdoid tumors to glutamine inhibition with 6-diazo-5-oxo-l-norleucine. Clin. Cancer Res, 2019, 25(19), 5925–5936. 10.1158/1078-0432.CCR-19-0189 PMID: 31300448 [PubMed: 31300448]

[13]. Leone RD; Zhao L; Englert JM; Sun IM; Oh MH; Sun IH; Arwood ML; Bettencourt IA; Patel CH; Wen J; Tam A; Blosser RL; Prchalova E; Alt J; Rais R; Slusher BS; Powell JD Glutamine blockade induces divergent metabolic programs to overcome tumor immune evasion. Science, 2019, 366(6468), 1013–1021. 10.1126/science.aav2588 PMID: 31699883 [PubMed: 31699883]

[14]. Sharma NS; Gupta VK; Garrido VT; Hadad R; Durden BC; Kesh K; Giri B; Ferrantella A; Dudeja V; Saluja A; Banerjee S Targeting tumor-intrinsic hexosamine biosynthesis sensitizes pancreatic cancer to anti-PD1 therapy. J. Clin. Invest, 2020, 130(1), 451–465. 10.1172/JCI127515 PMID: 31613799 [PubMed: 31613799]

[15]. Lemberg KM; Zhao L; Wu Y; Veeravalli V; Alt J; Aguilar JMH; Dash RP; Lam J; Tenora L; Rodriguez C; Nedelcovych MT; Brayton C; Majer P; Blakeley JO; Rais R; Slusher BS The novel glutamine antagonist prodrug JHU395 has antitumor activity in malignant peripheral nerve sheath tumor. Mol. Cancer Ther, 2020, 19(2), 397–408. 10.1158/1535-7163.MCT-19-0319 PMID: 31594823 [PubMed: 31594823]

[16]. Tcyganov E; Mastio J; Chen E; Gabrilovich DI Plasticity of myeloid-derived suppressor cells in cancer. Curr. Opin. Immunol, 2018, 51, 76–82. 10.1016/j.coi.2018.03.009 PMID: 29547768 [PubMed: 29547768]

[17]. Oh M-H; Sun IH; Zhao L; Leone RD; Sun IM; Xu W; Collins SL; Tam AJ; Blosser RL; Patel CH; Englert JM; Arwood ML; Wen J; Chan-Li Y; Tenora L; Majer P; Rais R; Slusher BS; Horton MR; Powell JD Targeting glutamine metabolism enhances tumor-specific immunity by modulating suppressive myeloid cells. J. Clin. Invest, 2020, 130(7), 3865–3884. 10.1172/JCI131859 PMID: 32324593 [PubMed: 32324593]

[18]. Cervantes-Madrid D; Romero Y; Duenas-Gonzalez A Reviving lonidamine and 6-diazo-5-oxo-l-norleucine to be used in combination for metabolic cancer therapy. BioMed Res. Int, 2015, 2015, 690492. 10.1155/2015/690492 PMID: 26425550 [PubMed: 26425550]

[19]. Alt J; Potter MC; Rojas C; Slusher BS Bioanalysis of 6-diazo-5-oxo-l-norleucine in plasma and brain by ultra-performance liquid chromatography mass spectrometry. Anal. Biochem, 2015, 474, 28–34. 10.1016/j.ab.2015.01.001 PMID: 25584882 [PubMed: 25584882]

[20]. Clasquin MF; Melamud E; Rabinowitz JD LC-MS data processing with MAVEN: A metabolomic analysis and visualization engine. Curr. Protoc. Bioinform, 2012, 37(1), 14.11.1–14.11.23. 10.1002/0471250953.bi1411s37

[21]. Thakare R; Chhonker YS; Gautam N; Alamoudi JA; Alnouti Y Quantitative analysis of endogenous compounds. J. Pharm. Biomed. Anal, 2016, 128, 426–437. 10.1016/j.jpba.2016.06.017 PMID: 27344632 [PubMed: 27344632]

[22]. Strassburg K; Huijbrechts AM; Kortekaas KA; Lindeman JH; Pedersen TL; Dane A; Berger R; Brenkman A; Hankemeier T; van Duynhoven J; Kalkhoven E; Newman JW; Vreeken RJ Quantitative profiling of oxylipins through comprehensive LC-MS/MS analysis: application in cardiac surgery. Anal. Bioanal. Chem, 2012, 404(5), 1413–1426. 10.1007/s00216-012-6226-x PMID: 22814969 [PubMed: 22814969]

[23]. Magill GB; Myers WP; Reilly HC; Putnam RC; Magill JW; Sykes MP; Escher GC; Karnofsky DA; Burchenal JH Pharmacological and initial therapeutic observations on 6-diazo-5-oxo-1-norleucine (DON) in human neoplastic disease. Cancer, 1957, 10(6), 1138–1150. 10.1002/1097-0142(195711/12)10:6<1138::AIDCNCR2820100608>3.0.CO;2-K PMID: 13489662 [PubMed: 13489662]

[24]. Earhart RH; Amato DJ; Chang AY; Borden EC; Shiraki M; Dowd ME; Comis RL; Davis TE; Smith TJ Phase II trial of 6- diazo-5-oxo-L-norleucine versus aclacinomycin-A in advanced sarcomas and mesotheliomas. Invest. New Drugs, 1990, 8(1), 113–119. 10.1007/BF00216936 PMID: 2188926 [PubMed: 2188926]

[25]. Rahman A; Smith FP; Luc PT; Woolley PV Phase I study and clinical pharmacology of 6-diazo-5-oxo-L-norleucine (DON). Invest. New Drugs, 1985, 3(4), 369–374. 10.1007/BF00170760 PMID: 4086244 [PubMed: 4086244]

[26]. DeWald HA; Moore AM 6-diazo-5-oxo-l-norleucine, a new tumor-inhibitory substance.1a preparation of l-, d- and dl-forms1b. J. Am. Chem. Soc, 1958, 80(15), 3941–3945. 10.1021/ja01548a036

[27]. Li MC; Whitmore WF Jr; Golbey R; Grabstald H Effects of combined drug therapy on metastatic cancer of the testis. JAMA, 1960, 174, 1291–1299. 10.1001/jama.1960.03030100059013 PMID: 13761819 [PubMed: 13761819]

[28]. A clinical study of the comparative effect of nitrogen mustard and DON in patients with bronchogenic carcinoma, Hodgkin's disease, lymphosarcoma, and melanoma. J. Natl. Cancer Inst, 1959, 22(2), 433–439. 10.1093/jnci/22.2.433 PMID: 13631504 [PubMed: 13631504]

[29]. Sullivan MP; Beatty EC Jr; Hyman CB; Murphy ML; Pierce MI; Severo NC A comparison of the effectiveness of standard dose 6-mercaptopurine, combination 6-mercaptopurine and DON, and high-loading 6-mercaptopurine therapies in treatment of the acute leukemias of childhood: results of a coperative study. Cancer Chemother. Rep, 1962, 18, 83–95. PMID: 13918321 [PubMed: 13918321]

[30]. Eagan RT; Frytak S; Nichols WC; Creagan ET; Ingle JN Phase II study on DON in patients with previously treated advanced lung cancer. Cancer Treat. Rep, 1982, 66(8), 1665–1666. PMID: 6286122 [PubMed: 6286122]

[31]. Lemberg KM; Vornov JJ; Rais R; Slusher BS We're not "don" yet: Optimal dosing and prodrug delivery of 6-diazo-5-oxo-l-norleucine. Mol. Cancer Ther, 2018, 17(9), 1824–1832. 10.1158/1535-7163.MCT-17-1148 PMID: 30181331 [PubMed: 30181331]

[32]. Yamashita AS; da Costa Rosa M; Stumpo V; Rais R; Slusher BS; Riggins GJ The glutamine antagonist prodrug JHU-083 slows malignant glioma growth and disrupts mTOR signaling. Neurooncol. Adv, 2020, 3(1), a149. 10.1093/noajnl/vdaa149 PMID: 33681764

[33]. Hanaford AR; Alt J; Rais R; Wang SZ; Kaur H; Thorek DLJ; Eberhart CG; Slusher BS; Martin AM; Raabe EH Orally bioavailable glutamine antagonist prodrug JHU-083 penetrates mouse brain and suppresses the growth of MYC-driven medulloblastoma. Transl. Oncol, 2019, 12(10), 1314–1322. 10.1016/j.tranon.2019.05.013 PMID: 31340195 [PubMed: 31340195]

[34]. Baresova V; Krijt M; Skopova V; Souckova O; Kmoch S; Zikanova M CRISPR-Cas9 induced mutations along *de novo* purine synthesis in HeLa cells result in accumulation of individual enzyme substrates and affect purinosome formation. Mol. Genet. Metab, 2016, 119(3), 270–277. 10.1016/j.ymgme.2016.08.004 PMID: 27590927 [PubMed: 27590927]

[35]. Krijt M; Souckova O; Baresova V; Skopova V; Zikanova M Metabolic tools for identification of new mutations of enzymes engaged in purine synthesis leading to neurological impairment. Folia Biol. (Praha), 2019, 65(3), 152–157. PMID: 31638562 [PubMed: 31638562]

[36]. Bagnara AS; Letter AA; Henderson JF Multiple mechanisms of regulation of purine biosynthesis *de novo* in intact tumor cells. Biochim. Biophys. Acta, 1974, 374(3), 259–270. 10.1016/0005-2787(74)90247-0 PMID: 4373080 [PubMed: 4373080]

[37]. Jones BR; Schultz GA; Eckstein JA; Ackermann BL Surrogate matrix and surrogate analyte approaches for definitive quantitation of endogenous biomolecules. Bioanalysis, 2012, 4(19), 2343–2356. 10.4155/bio.12.200 PMID: 23088461 [PubMed: 23088461]

[38]. Ho S; Gao H Surrogate matrix: opportunities and challenges for tissue sample analysis. Bioanalysis, 2015, 7(18), 2419–2433. 10.4155/bio.15.161 PMID: 26395421 [PubMed: 26395421]

[39]. Fan TWM; Lorkiewicz PK; Sellers K; Moseley HN; Higashi RM; Lane AN Stable isotope-resolved metabolomics and applications for drug development. Pharmacol. Ther, 2012, 133(3), 366–391. 10.1016/j.pharmthera.2011.12.007 PMID: 22212615 [PubMed: 22212615]

[40]. Parker SL; Pandey S; Sime FB; Stuart J; Lipman J; Roberts JA; Wallis SC A validated LC-MS/MS method for the simultaneous quantification of the novel combination antibiotic, ceftolozane-tazobactam, in plasma (total and unbound), CSF, urine and renal replacement therapy effluent: application to pilot pharmacokinetic studies. Clin. Chem. Lab. Med, 2020, 59(5), 921–933. 10.1515/cclm-2020-1196 PMID: 33554515 [PubMed: 33554515]

[41]. Tan A; Awaiye K; Trabelsi F Impact of calibrator concentrations and their distribution on accuracy of quadratic regression for liquid chromatography-mass spectrometry bioanalysis. Anal. Chim. Acta, 2014, 815, 33–41. 10.1016/j.aca.2014.01.036 PMID: 24560370 [PubMed: 24560370]

[42]. Gu H; Liu G; Wang J; Aubry AF; Arnold ME Selecting the correct weighting factors for linear and quadratic calibration curves with least-squares regression algorithm in bioanalytical LC-MS/MS assays and impacts of using incorrect weighting factors on curve stability, data quality, and assay performance. Anal. Chem, 2014, 86(18), 8959–8966. 10.1021/ac5018265 PMID: 25157966 [PubMed: 25157966]

[43]. Park HY; Kim MJ; Lee S; Jin J; Lee S; Kim JG; Choi YK; Park KG Inhibitory effect of a glutamine antagonist on proliferation and migration of VSMCs via simultaneous attenuation of glycolysis and oxidative phosphorylation. Int. J. Mol. Sci, 2021, 22(11), 5602. 10.3390/ijms22115602 PMID: 34070527 [PubMed: 34070527]

[44]. Pham K; Maxwell MJ; Sweeney H; Alt J; Rais R; Eberhart CG; Slusher BS; Raabe EH Novel glutamine antagonist JHU395 suppresses MYC-driven medulloblastoma growth and induces apoptosis. J. Neuropathol. Exp. Neurol, 2021, 80(4), 336–344. 10.1093/jnen/nlab018 PMID: 33712838 [PubMed: 33712838]

[45]. Lemberg KM Abstract 1293: A novel protide purine antimetabolite combines with the prodrug glutamine antagonist JHU395 in preclinical models of Ras-driven sarcomas. Cancer Res, 2021, 81(13)(Suppl.), 1293. [PubMed: 33376114]

[46]. Johnson ML Phase 1 and phase 2a, first-in-human (FIH) study, of DRP-104, a broad glutamine antagonist, in adult patients with advanced solid tumors. J. Clin. Oncol., 2021, 39(15)(Suppl.), TPS3149–TPS3149. 10.1200/JCO.2021.39.15_suppl.TPS3149

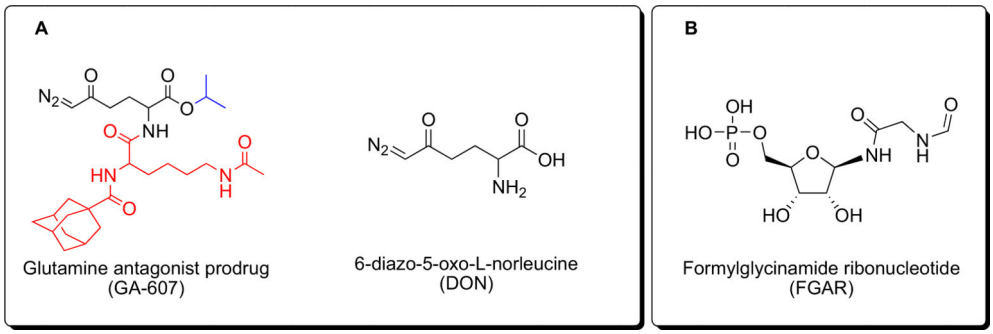

Fig. (1).
Molecular structures of (**A**) GA-607, DON, and (**B**) FGAR.

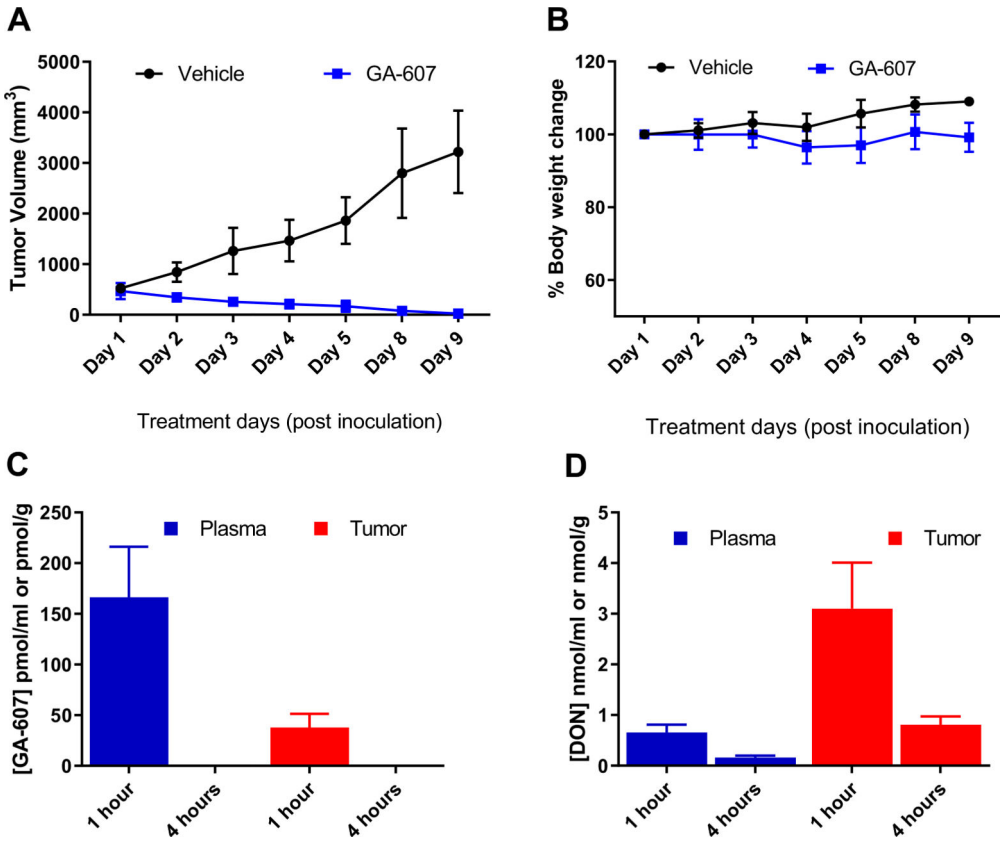

Fig. (2).

Efficacy, tolerability, and pharmacokinetic assessment of GA-607 in EL4 tumor-bearing mice following GA-607 (3.2 mg/kg SC) treatment; dosed 5 consecutive days followed by 2 drug-free days. Tumors volumes and body weights were only measured on the day of dosing. (**A**) Complete tumor regression was observed following GA-607 administration. (**B**) No change in body weight was observed following GA-607 administration. (**C**) GA-607 and (**D**) GA-607-derived DON levels in plasma and tumors following GA-607 administration.

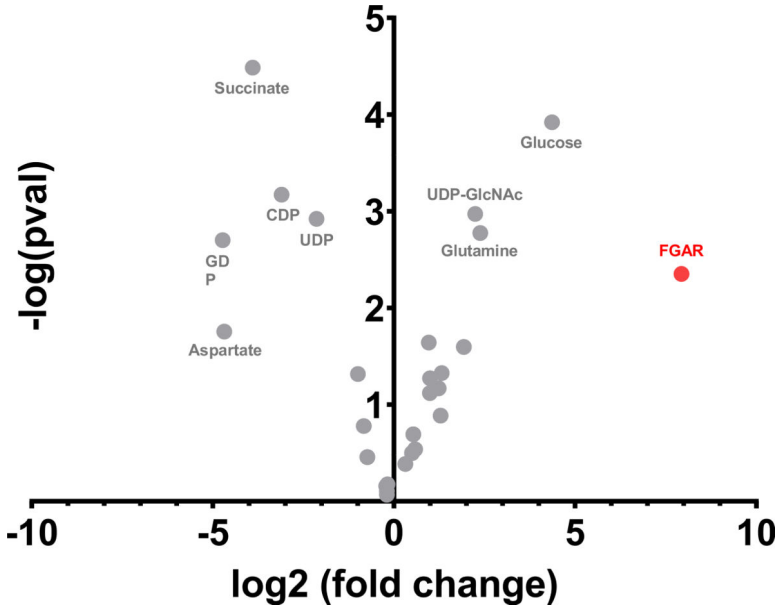

Fig. (3).

Metabolomic analysis of GA-607-*versus* vehicle-treated EL4 tumors. GA-607 treatment caused an increase in FGAR, glucose, glutamine, and uridine 5′-diphospho-*N*-acetylglucosamine in the tumor and a decrease in succinate, aspartate, and nucleotide diphosphates.

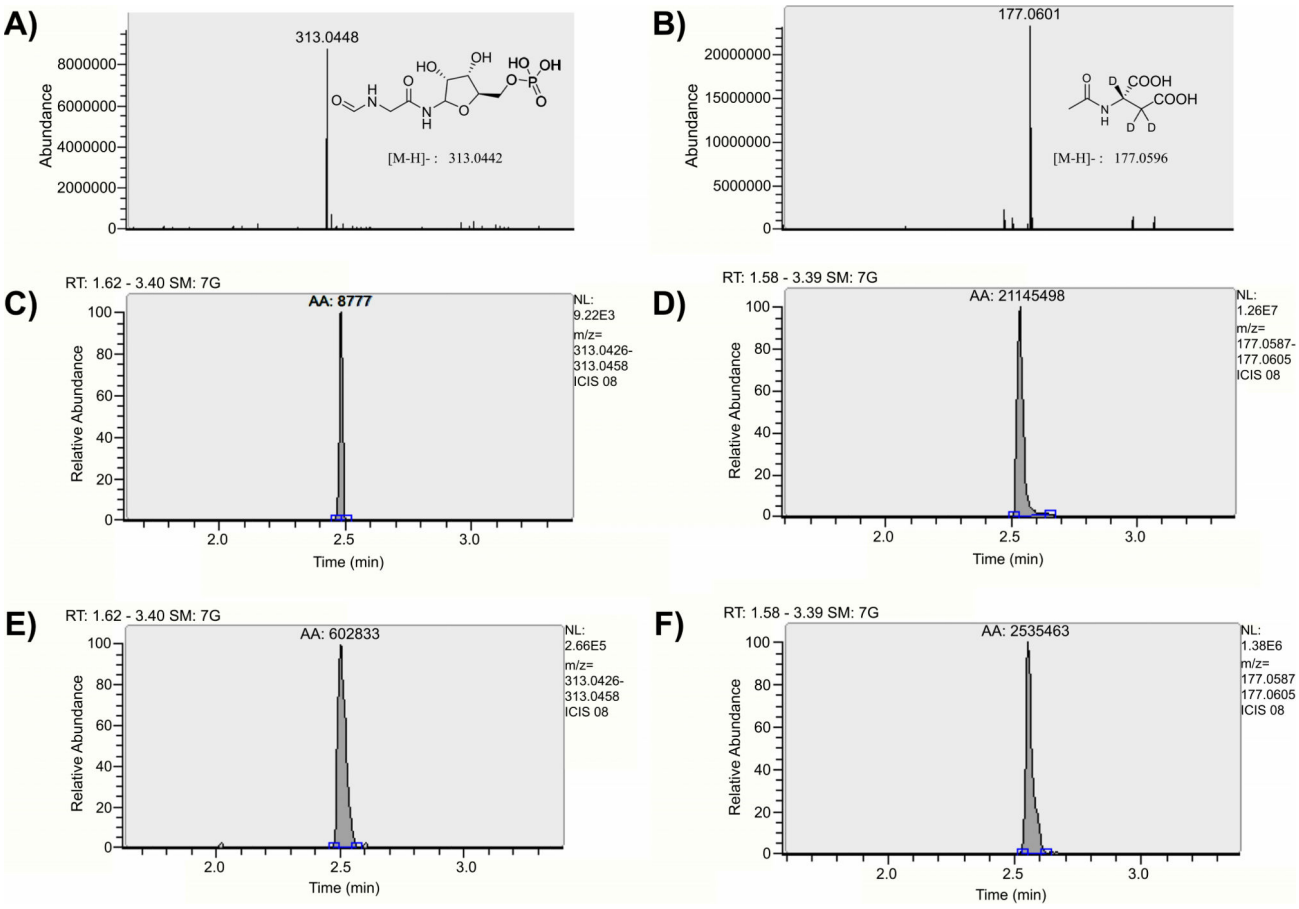

Fig. (4).

Representative high-resolution mass spectrum and chromatographic spectra of FGAR and IS. (**A**) High-resolution full scan mass spectrum of FGAR in negative mode with < 2 ppm error; (**B**) high-resolution full scan mass spectrum of internal standard (NAA-d_3) in negative mode with < 2 ppm error; (**C**) extracted chromatogram of FGAR spiked in plasma at LLOQ (0.03 nmol/mL); (**D**) extracted chromatogram for internal standard (NAA-d_3) in plasma; (**E**) extracted chromatogram of FGAR spiked in tumor at LLOQ (1 nmol/g); (**F**) extracted chromatogram for internal standard (NAA-d_3) in EL4 tumor.

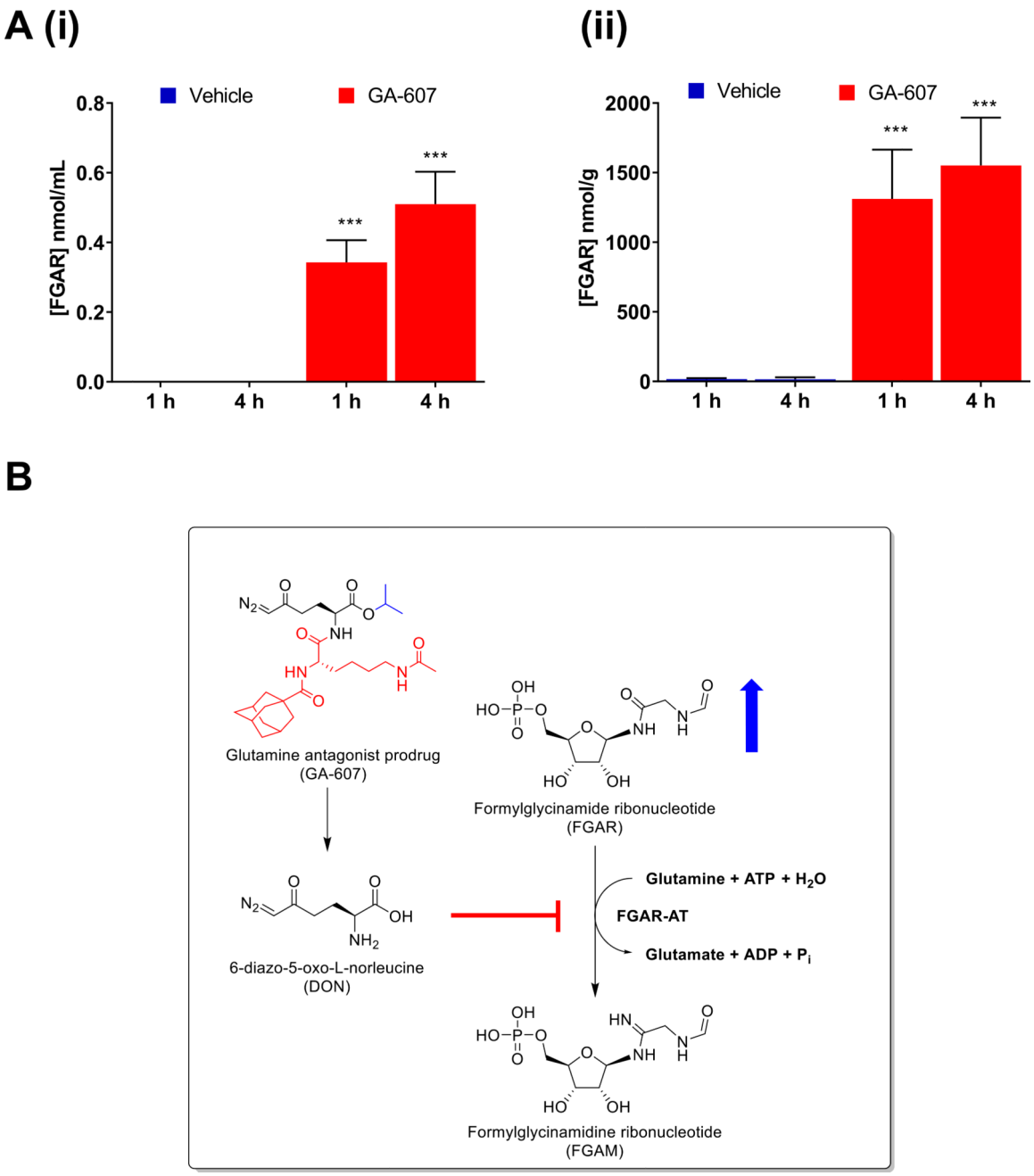

Fig. (5).

FGAR quantification following GA-607 treatment (3.2 mg/kg SC daily for 4 days) in EL4 tumor-bearing mice. **(A)** (i) FGAR levels in plasma at 1 and 4 hours after GA-607 or vehicle administration; (ii) FGAR levels in tumor at 1 and 4 hours after GA-607 or vehicle administration. Mean ± S.D. ***p > .001 (two-way ANOVA with Tukey's post hoc test) (**B**) Schematic representation of the biochemical pathway regulating FGAR metabolism in tumor tissues and the effect of GA therapy. FGAR-AT, an enzyme in *de novo* purine synthesis catalyzes the conversion of FGAR, ATP, and glutamine to FGAM, ADP, Pi, ammonia, and

glutamate, respectively. Upon cleavage in tumors, GA-607 releases DON. The inhibition of FGAR-AT results in elevated FGAR levels.

Table 1.

Statistical evaluation of calculated concentrations of FGAR obtained from the calibration curves (n=3) prepared in mouse plasma and mouse tumor homogenates.

Mouse Plasma			Mouse Tumor Homogenate		
Nominal Conc. (nmol/mL)	**Accuracy (%)**	**Precision (% RSD)**	**Nominal Conc. (nmol/g)**	**Accuracy (%)**	**Precision (% RSD)**
100	94.4	5.18	10000	98.9	0.46
32.0	103	8.64	3000	102	1.21
10.0	98.9	6.76	1000	102	1.51
3.20	105	5.31	300	101	1.74
1.00	98.6	4.63	100	100	3.27
0.32	97.1	10.3	30	104	1.32
0.10	100	9.05	10	95.9	1.31
0.03	101	7.10	3	93.0	4.83
-	-	-	1	103	1.52

Table 2.

Stability of FGAR in mouse plasma after subjecting to 3 freeze-thaw cycles, bench-top (6 h at room temperature), and long-term conditions (−80°C for 4 weeks) before extraction and autosampler (18 h at 4°C) after extraction.

Nominal Conc. (nmol/mL)	Stability (%)			
	Freeze-thaw	Bench-top	Long-term	Autosampler
80.0	107 ± 3.57	100 ± 5.32	96.5 ± 2.12	95.2 ± 2.40
2.00	114 ± 7.84	91.9 ± 6.22	86.5 ± 6.72	96.4 ± 0.591
0.08	112 ± 5.14	96.0 ± 12.1	92.5 ± 11.2	101 ± 8.88

Table 3.

Stability of FGAR in mouse tumor homogenates after subjecting to 3 freeze-thaw cycles, bench-top (6 h at room temperature), and long-term conditions (−80°C for 4 weeks) before extraction and autosampler (18 h at 4°C) after extraction.

Nominal Conc. (nmol/mL)	Stability (%)			
	Freeze-Thaw	Bench-Top	Long-Term	Autosampler
2000	104 ± 3.76	102 ± 3.17	113 ± 2.31	103 ± 0.02
200	93.5 ± 3.95	106 ± 4.31	110 ± 3.85	102 ± 0.00
20	104 ± 2.59	109 ± 7.93	96.2 ± 2.79	107 ± 0.06

Table 4.

Accuracy and precision in mouse plasma.

Nominal Conc. (nmol/mL)	Intra-day (n=3)		Inter-day (n=6)	
	Accuracy (%)	Precision (% RSD)	Accuracy (%)	Precision (% RSD)
80.0	95.8	3.96	99.4	4.82
2.00	92.0	4.19	98.9	9.39
0.08	111	10.6	91.0	13.6

Inter and intra–day precision and accuracy for FGAR in plasma were determined by analyzing replicates (n=3/day) of spiked samples at 3 different concentration levels over 2 subsequent days. Statistics for inter-day evaluation are generated from n=6 samples.

Table 5.

Accuracy and precision in mouse tumor homogenates.

Nominal Conc. (nmol/g)	Intra-day (n=3)		Inter-day (n=6)	
	Accuracy (%)	Precision (% RSD)	Accuracy (%)	Precision (% RSD)
2000	96.8	3.05	98.1	4.03
200	101	3.39	104	4.11
20	95.2	1.69	98.2	6.03

Inter and intra-day precision and accuracy for FGAR in EL4 tumor homogenates were determined by analyzing replicates (n=3/day) of spiked samples at 3 different concentration levels over 2 subsequent days. Statistics for inter-day evaluation are generated from n=6 samples.